NATIONAL ADVISORY COMMITTEE FOR AERONAUTICS

TECHNICAL NOTE 4350

THEORETICAL DISTRIBUTION OF LAMINAR-BOUNDARY-LAYER THICKNESS, BOUNDARY-LAYER REYNOLDS NUMBER AND STABILITY LIMIT, AND ROUGHNESS REYNOLDS NUMBER FOR A SPHERE AND DISK IN INCOMPRESSIBLE FLOW

By Neal Tetervin

Langley Aeronautical Laboratory
Langley Field, Va.

Washington

September 1958

NACA TN 4276

By Dean R. Chapman
May 1958

In figure 16 change Eq. (69) to read Eq. (56).

Change C_D to read $(C_D)_{L/D = 0}$ where it appears in:

Ordinates of figures 17 and 19

Line 5 from bottom on page 33

Lines 3 and 4 from top on page 34

Issued 9-19-58

NATIONAL ADVISORY COMMITTEE FOR AERONAUTIC

TECHNICAL NOTE 4350

THEORETICAL DISTRIBUTION OF LAMINAR-BOUNDARY-LAYER THICKNESS, BOUNDARY-LAYER REYNOLDS NUMBER AND STABILITY LIMIT, AND ROUGHNESS REYNOLDS NUMBER FOR A SPHERE AND DISK IN INCOMPRESSIBLE FLOW

By Neal Tetervin

SUMMARY

The laminar-boundary-layer thickness, the boundary-layer Reynolds number and minimum critical Reynolds number, and the roughness Reynolds number have been calculated by an approximate method for a sphere and disk in the supercritical Reynolds number region. The calculations for the sphere show that the boundary layer at the stagnation point of a sphere is much thicker than that on an airfoil, that the boundary-layer thickness increases very slowly with an increase in distance from the stagnation point, that the boundary layer over the forward portion of a sphere is highly stable at large Reynolds numbers with respect to the Tollmien-Schlichting type of waves, and that roughness of a given height produces the largest roughness Reynolds numbers at about 57° from the stagnation point. The calculations for the disk show the unusual result that the boundary-layer thickness is greatest at the stagnation point and decreases with an increase in distance from this point, that the boundary layer is extremely stable with respect to the Tollmien-Schlichting type of waves, and that roughness of a given height produces a given roughness Reynolds number over a smaller portion of the disk surface than over the sphere surface.

INTRODUCTION

In connection with an experimental subsonic-speed investigation undertaken recently at the Langley Aeronautical Laboratory of the transition from laminar to turbulent flow on a sphere at a Reynolds number of 4.7×10^6, based on a radius of 60 inches, the thickness of the laminar boundary layer, its stability, and the roughness Reynolds numbers for various-sized roughness particles were calculated by approximate methods

for incompressible flow. In addition to the calculations for a sphere, calculations were also made for a much blunter body, namely, for a disk with a radius of 60 inches perpendicular to the flow at a Reynolds number of 4.7×10^6.

Some time after the calculations were completed it was discovered that measured transition positions on a 9-inch-radius sphere had been reported in reference 1 up to a Reynolds number of 1.75×10^6, based on the radius. Calculated distributions of the boundary-layer momentum thickness over the forward portion of the sphere for six Reynolds numbers between 0.5×10^6 and 3×10^6 as well as the position of the neutral-stability point up to a Reynolds number of 3×10^6 were also presented in reference 1.

In the present paper the calculated distribution of the boundary-layer momentum thickness over the forward portion of a sphere is presented in the form of a single nondimensional curve that allows the thickness at any Reynolds number to be obtained with almost no calculation. The calculated boundary-layer Reynolds numbers at any value of the sphere Reynolds number can also be readily obtained from a single curve. The distribution of the minimum critical Reynolds number on the sphere, which is independent of the sphere Reynolds number, is presented as well as the location of the neutral-stability point for Reynolds numbers up to $1{,}000 \times 10^6$. Finally, the distribution over the sphere of a nondimensional roughness parameter that allows the roughness Reynolds number to be quickly calculated for any small roughness height at any value of the sphere Reynolds number is shown in the form of a single curve.

The calculated results are for the supercritical Reynolds number range, that is, for the range in which the final separation of the boundary layer on the sphere is that of the turbulent boundary layer. In this range the pressure distribution over the forward portion of the sphere is almost independent of the Reynolds number, and, thus, the present calculations are good approximations for any sphere at any supercritical Reynolds number.

Most of the calculated quantities presented for the sphere are also presented in the same form for the disk.

SYMBOLS

a,A,b,C,d,e	constants
$\bar{c}$	reference length, radius of sphere or disk

F' velocity ratio, $\bar{u}/\bar{U}$ (eq. (15) of ref. 2)

$$f = \frac{\bar{\tau}_w \bar{\theta}}{\bar{\mu}\bar{U}}$$

$$f_1 = -\frac{\bar{v}_w}{\bar{U}_\infty}\sqrt{\frac{\bar{U}_\infty \bar{c}}{\bar{\nu}}}$$

$$g = \frac{\bar{\theta}}{\bar{\delta}_1}$$

$$h = \frac{\bar{h}}{\bar{c}}$$

$\bar{h}$ height of roughness particle

K Schlichting velocity-profile shape parameter

$$k = \frac{\bar{\theta}^2}{\bar{\nu}}\frac{d\bar{U}}{d\bar{x}} = Z\frac{dU}{dx}$$

$$k_1 = -\frac{\bar{v}_w \bar{\theta}}{\bar{\nu}} = -\frac{v_w}{U} R_\theta = f_1\sqrt{Z}$$

R_c reference Reynolds number, $\bar{U}_\infty \bar{c}/\bar{\nu}$

R_h roughness Reynolds number, $\bar{u}_h \bar{h}/\bar{\nu}$

$$R_\theta = \frac{\bar{U}\bar{\theta}}{\bar{\nu}}$$

$R_{\theta,c}$ minimum critical Reynolds number, value of R_θ at which a small disturbance is neither damped nor amplified

$$r = \frac{\bar{r}}{\bar{c}}$$

$\bar{r}$ perpendicular distance from point on surface of body of revolution to axis of symmetry

$$U = \frac{\bar{U}}{\bar{U}_\infty}$$

$\bar{U}$ velocity at outer edge of boundary layer and in direction of $\bar{x}$

$\bar{U}_\infty$ free-stream velocity

$u = \frac{\bar{u}}{\bar{U}_\infty}$

$\bar{u}$ velocity inside boundary layer and in direction of $\bar{x}$

$\bar{u}_h$ velocity at $\bar{y} = \bar{h}$ with roughness particle absent

$v_w = \frac{\bar{v}_w}{\bar{U}_\infty}$

$\bar{v}_w$ velocity through surface, positive outward

$x = \frac{\bar{x}}{\bar{c}}$ (For a sphere, $\bar{x}/\bar{c}$ is equal to the angle in radians from the stagnation point)

Δx increment in x

x_o initial station of x

$\bar{x}$ distance along surface, measured from stagnation point

Y nondimensional distance from surface (ref. 2)

$y = \frac{\bar{y}}{\bar{c}}$

$\bar{y}$ distance normal to surface, positive outward

$Z = \theta^2 R_c$

β wedge-angle parameter

$\beta_1 = Zr^2$

δ^* displacement thickness, $\bar{\delta}^*/\bar{c}$

$\bar{\delta}^* = \int_0^\infty \left(1 - \frac{\bar{u}}{\bar{U}}\right) d\bar{y}$

$\bar{\delta}_1$ measure of boundary-layer thickness (ref. 3)

θ momentum thickness, $\bar{\theta}/\bar{c}$

$$\bar{\theta} = \int_0^{\infty} \frac{\bar{u}}{\bar{U}}\left(1 - \frac{\bar{u}}{\bar{U}}\right)d\bar{y}$$

$\bar{\mu}$ viscosity of fluid

$\bar{\nu}$ kinematic viscosity, $\bar{\mu}/\bar{\rho}$

$\bar{\rho}$ density of fluid

$\bar{\tau}_w$ surface shearing stress

Subscripts:

a actual

d disk

o initial point

p plate

t stagnation point

th theoretical

w surface

Barred quantities are dimensional.

ANALYSIS AND DISCUSSION

Sphere

The boundary-layer characteristics for a sphere were calculated by use of the modified Schlichting method (ref. 4) which was altered to apply to a body of revolution. (See ref. 3 for the original method.) The change from the method for two-dimensional flow consists in using the momentum equation for a body of revolution instead of the momentum equation for two-dimensional flow. The momentum equation for the flow over a body of revolution (see ref. 5) is

$$\frac{d\bar{\theta}}{d\bar{x}} + \frac{\bar{\theta}}{\bar{U}}\frac{d\bar{U}}{d\bar{x}}\left(2 + \frac{\bar{\delta}^*}{\bar{\theta}}\right) + \frac{\bar{\theta}}{\bar{r}}\frac{d\bar{r}}{d\bar{x}} - \frac{\bar{v}_w}{\bar{U}} = \frac{\bar{\tau}_w}{\bar{\rho}\bar{U}^2} \tag{1}$$

When the following three quantities

$$k = \frac{\bar{\theta}^2}{\bar{\nu}}\frac{d\bar{U}}{d\bar{x}} = \left(\frac{\bar{\theta}}{\bar{c}}\right)^2 \frac{d\,\frac{\bar{U}}{\bar{U}_\infty}}{d\,\frac{\bar{x}}{\bar{c}}}\frac{\bar{U}_\infty \bar{c}}{\bar{\nu}} = \theta^2 \frac{dU}{dx} R_c = Z\frac{dU}{dx} \qquad \left(Z = \theta^2 R_c\right)$$

$$k_1 = -\frac{\bar{v}_w \bar{\theta}}{\bar{\nu}} = -\frac{\bar{v}_w}{\bar{U}_\infty}\frac{\bar{\theta}}{\bar{c}}\frac{\bar{U}_\infty \bar{c}}{\bar{\nu}} = -v_w \theta R_c = f_1\sqrt{Z}$$

and

$$f = \frac{\bar{\tau}_w \bar{\theta}}{\bar{U}\bar{\mu}} = \frac{\bar{\tau}_w}{\bar{\rho}\bar{U}^2} R_\theta$$

from reference 4 are introduced into equation (1), the result is

$$\frac{dZ}{dx} = \frac{2}{U}\left[f - k_1 - k\left(2 + \frac{\delta^*}{\theta}\right)\right] - \frac{2Z}{r}\frac{dr}{dx} \tag{2}$$

Introducing the quantity $\beta_1 = Zr^2$ into equation (2) gives

$$\frac{d\beta_1}{dx} = \frac{2r^2}{U}\left[f - k_1 - k\left(2 + \frac{\delta^*}{\theta}\right)\right] \tag{3}$$

In order to find $\beta_1(x)$, equation (3) can be written as

$$\beta_1 = 2\int_0^x \frac{r^2}{U}\left[f - k_1 - k\left(2 + \frac{\delta^*}{\theta}\right)\right]dx + \beta_{1,o} \tag{4}$$

where $\beta_{1,o} = 0$ because $\beta_1 = Zr^2$; and at $x = 0$ the quantity Z is finite and $r = 0$.

In order to integrate equation (4), Simpson's rule (see ref. 6) was used to obtain

$$\beta_1 = (\beta_1)_{x-2\Delta x} + \frac{2\,\Delta x}{3}\left(\left\{\frac{r^2}{U}\left[f - k_1 - k\left(2 + \frac{\delta^*}{\theta}\right)\right]\right\}_{x-2\Delta x} + 4\left\{\frac{r^2}{U}\left[f - k_1 - k\left(2 + \frac{\delta^*}{\theta}\right)\right]\right\}_{x-\Delta x} + \left\{\frac{r^2}{U}\left[f - k_1 - k\left(2 + \frac{\delta^*}{\theta}\right)\right]\right\}_{x}\right) \quad (5)$$

Equation (5) can be solved by iteration; the first approximation for the expression $\left\{\frac{r^2}{U}\left[f - k_1 - k\left(2 + \frac{\delta^*}{\theta}\right)\right]\right\}_x$ is obtained by extrapolation of β_1 from the values at smaller values of x. Near the stagnation point, sufficient values for applying this method of integration are obtained by the process described in the immediately following paragraph. When β_1 and, thus, Z are known at any value of x, the quantities f, k_1, k, and δ^*/θ at that value of x can be calculated or read from charts. (See refs. 3 and 4.)

In order to begin the integration at the stagnation point, equation (2) is written as

$$\frac{dZ}{dx} = \frac{2}{U}\left\{\left[f - k_1 - k\left(2 + \frac{\delta^*}{\theta}\right)\right] - \frac{ZU}{r}\frac{dr}{dx}\right\} \quad (6)$$

and use is made of the fact that, near the stagnation point, $r = x$ and $U = \left(\frac{dU}{dx}\right)_t x$. The term $\frac{ZU}{r}\frac{dr}{dx}$ in equation (6) then becomes

$$\frac{ZU}{r}\frac{dr}{dx} = \frac{Z\left(\frac{dU}{dx}\right)_t x}{x} = Z\left(\frac{dU}{dx}\right)_t = \left[Z_t + \left(\frac{dZ}{dx}\right)_t x\right]\left(\frac{dU}{dx}\right)_t$$

or

$$\frac{ZU}{r}\frac{dr}{dx} = k_t + \left(\frac{dZ}{dx}\right)_t\left(\frac{dU}{dx}\right)_t x$$

Equation (6) can then be written as

$$\frac{dZ}{dx} = \frac{2}{U}\left[f - k_1 - k\left(2 + \frac{\delta^*}{\theta}\right) - k_t\right] - \frac{2\left(\frac{dZ}{dx}\right)_t \left(\frac{dU}{dx}\right)_t x}{U}$$

which, upon noting that $U = \left(\frac{dU}{dx}\right)_t x$ near $x = 0$, gives

$$3\left(\frac{dZ}{dx}\right)_t = \lim_{x \to 0} \frac{2\left[f - k_1 - k\left(2 + \frac{\delta^*}{\theta}\right) - k_t\right]}{U} \tag{7}$$

Because $U = 0$ at $x = 0$, it is necessary that

$$\left[f - k_1 - k\left(3 + \frac{\delta^*}{\theta}\right)\right]_t = 0 \tag{8}$$

in order that $\left(\frac{dZ}{dx}\right)_t$ be finite.

Equation (8) together with the relation

$$g^2(K + 1) - fk_1 - k = 0 \tag{9}$$

from reference 4 can be used to determine the initial values of K, k, and k_1 when $v_{w,t}$, $\left(\frac{dU}{dx}\right)_t$, and R_c are known by the same method used for two-dimensional flow in reference 4. The quantity K is the parameter that determines the shape of the velocity profile; g is a ratio of two boundary-layer thicknesses and depends on K only. In the present calculations $k_1 = 0$, and, thus, equations (8) and (9) reduce to

$$\left[g^2(K + 1)\left(3 + \frac{\delta^*}{\theta}\right) - f\right]_t = 0 \tag{10}$$

Because f, g, and δ^*/θ depend only on the velocity-profile shape parameter K, equation (10) can be solved numerically for K_t and the value of k_t can then be calculated from equation (9) with $k_1 = 0$. The results are

$$K_t = -0.72542$$

$$k_t = 0.05299$$

The initial values of K_t and k_t are, thus, known; for the present case $f_1 = 0$ and, therefore, either K_t or k_t is sufficient to determine K, f, δ^*/θ, and g.

In order to begin the integration of equation (4), it is useful to know how β_1 varies near $x = 0$. This variation is obtained from equation (3) together with $r = x$, $U = \left(\frac{dU}{dx}\right)_t x$, and the fact that f, k_1, k, and δ^*/θ are finite. Then, it follows from equation (3) that $\frac{d\beta_1}{dx} = 0$ at $x = 0$. The second derivative $\frac{d^2\beta_1}{dx^2}$ at $x = 0$ can also be easily calculated; thus, near $x = 0$ equation (3) becomes

$$\frac{d\beta_1}{dx} = \frac{2x}{\left(\frac{dU}{dx}\right)_t}\left[f - k_1 - k\left(2 + \frac{\delta^*}{\theta}\right)\right]$$

Then,

$$\frac{d^2\beta_1}{dx^2} = \frac{2x}{\left(\frac{dU}{dx}\right)_t}\left[\frac{\partial f}{\partial k} - \left(2 + \frac{\delta^*}{\theta}\right) - k\,\frac{\partial \frac{\delta^*}{\theta}}{\partial k}\right]\frac{dk}{dx} -$$

$$\frac{2x}{\left(\frac{dU}{dx}\right)_t}\left[1 + k\,\frac{\partial \frac{\delta^*}{\theta}}{\partial k_1} - \frac{\partial f}{\partial k_1}\right]\frac{dk_1}{dx} + \frac{2}{\left(\frac{dU}{dx}\right)_t}\left[f - k_1 - k\left(2 + \frac{\delta^*}{\theta}\right)\right]$$

or

$$\left(\frac{d^2\beta_1}{dx^2}\right)_t = \frac{2}{\left(\frac{dU}{dx}\right)_t}\left[f - k_1 - k\left(2 + \frac{\delta^*}{\theta}\right)\right]_t$$

In order to obtain $\left(\frac{d^3\beta_1}{dx^3}\right)_t$ note that

$$\left(\frac{d^3\beta_1}{dx^3}\right)_t = \lim_{x \to 0} \frac{1}{x}\left[\frac{d^2\beta_1}{dx^2} - \left(\frac{d^2\beta_1}{dx^2}\right)_t\right]$$

The result obtained is $\left(\frac{d^3\beta_1}{dx^3}\right)_t = 0$ for $\frac{dk}{dx} = \frac{dk_1}{dx} = 0$ at $x = 0$, which

follows from the restrictions $\frac{df_1}{dx} = \frac{d^2r}{dx^2} = \frac{d^2U}{dx^2} = 0$ at $x = 0$.

Then, near $x = 0$,

$$\beta_1 = \beta_{1,t} + \left(\frac{d\beta_1}{dx}\right)_t x + \left(\frac{d^2\beta_1}{dx^2}\right)_t \frac{x^2}{2!} + \left(\frac{d^3\beta_1}{dx^3}\right)_t \frac{x^3}{3!} + \cdots$$

or, because $\beta_{1,t} = \left(\frac{d\beta_1}{dx}\right)_t = \left(\frac{d^3\beta_1}{dx^3}\right)_t = 0$,

$$\beta_1 = \frac{x^2}{\left(\frac{dU}{dx}\right)_t}\left[f - k_1 - k\left(2 + \frac{\delta^*}{\theta}\right)\right]_t + (\text{Error})\ O\left[x^4\right] \qquad (11)$$

The calculation of β_1 is begun by making use of equation (11) and is continued by use of equation (5) together with the relations $U = \frac{3}{2}\sin x$ and $r = \sin x$. (See p. 417 of ref. 7.)

The quantity Z is obtained from β_1 by the relation $Z = \frac{\beta_1}{r^2}$ which follows from the definition of β_1. By using the definition $k = Z\frac{dU}{dx}$, equation (11), the relation $Z = \frac{\beta_1}{r^2}$ where $r = x$, and equation (8), the subsequent relation results at the stagnation point:

$$Z_t = \frac{k_t}{\left(\frac{dU}{dx}\right)_t} \qquad (12)$$

All the calculations were made for a velocity distribution outside the boundary layer given by $U = \frac{3}{2}\sin x$, the potential-flow velocity distribution for a sphere. A comparison of the velocity distribution given by the expression $U = \frac{3}{2}\sin x$ with the measured velocity distributions (ref. 8) for the so-called supercritical range of Reynolds numbers shows that the expression $U = \frac{3}{2}\sin x$ is a good approximation for the experimental velocity distribution for most of the forward portion of the sphere and can be considered as the limiting distribution for the experimental velocity distributions.

The calculated variation of $\frac{\bar{\theta}}{\bar{c}}\sqrt{R_c}$ (or $\sqrt{Z}$) with $\bar{x}/\bar{c}$ is shown in figure 1. The presentation of the results in the form of $\frac{\bar{\theta}}{\bar{c}}\sqrt{R_c}$ plotted against $\bar{x}/\bar{c}$ enables the boundary-layer momentum thickness to be easily calculated for a sphere of any size and at any Reynolds number in the supercritical Reynolds number region. It is noted that the boundary-layer thickness increases very slowly with increase in distance from the stagnation point. This behavior differs from that on an airfoil (see p. 211 of ref. 9) on which the boundary-layer thickness increases rapidly from its value at the stagnation point. It is also noted that the value of $\frac{\bar{\theta}}{\bar{c}}\sqrt{R_c}$ at the stagnation point of the sphere is about 10 times as large as that at the stagnation point of the airfoil having an NACA 64A010 section at zero angle of attack.

In figure 2 is shown the variation with $\bar{x}/\bar{c}$ at $R_c = 4.7 \times 10^6$ of the boundary-layer Reynolds number R_θ and of the boundary-layer minimum critical Reynolds number $R_{\theta,c}$, the Reynolds number below which very small wave-like disturbances (Tollmien-Schlichting type of waves as discussed in ref. 9) are damped out. The Reynolds number R_θ is obtained from the relation

$$\begin{aligned} R_\theta &= \frac{\bar{U}\bar{\theta}}{\bar{\nu}} \\ &= \frac{\bar{U}}{\bar{U}_\infty}\frac{\bar{\theta}}{\bar{c}}\frac{\bar{U}_\infty \bar{c}}{\bar{\nu}} \\ &= U\theta R_c \\ &= \left(U\sqrt{R_c}\right)\left(\theta\sqrt{R_c}\right) \end{aligned} \tag{13}$$

Because U and $\theta\sqrt{R_c}$ are independent of R_c, it is apparent that R_θ is directly proportional to $\sqrt{R_c}$. Therefore, the value of R_θ at any value of R_c is obtained by using

$$\frac{R_\theta}{(R_\theta)_{R_c=4.7\times10^6}} = \sqrt{\frac{R_c}{4.7 \times 10^6}} \tag{14}$$

The minimum critical Reynolds number $R_{\theta,c}$ depends on the shape parameter K alone of the velocity profile. The values of $R_{\theta,c}$ are, therefore, obtained from figure 1 of reference 4. The parameter K is dependent only on the velocity distribution outside the boundary layer and is independent of R_c; therefore, $R_{\theta,c}$ is independent of R_c. Here, again, the behavior of R_θ and $R_{\theta,c}$ is different from that on an airfoil.

(See ref. 4.) For the sphere the value of R_θ increases linearly with $\bar{x}/\bar{c}$ for the smaller values of $\bar{x}/\bar{c}$. The values of $R_{\theta,c}$ remain almost constant at first and then decrease at an increasing rate. For the airfoil with an NACA 64A010 section and at zero angle of attack, R_θ increases in a parabolic manner with x; and $R_{\theta,c}$, after a sudden large drop from its value at the stagnation point, remains almost constant to the value of x where the pressure is at a minimum.

From equation (14) and figure 2 the value of R_c necessary for neutral stability $\left(R_\theta = R_{\theta,c}\right)$ at any value of $\bar{x}/\bar{c}$ can be calculated. The results are shown in figure 3. It is noted that at a Reynolds number of 4.7×10^6 the boundary layer is stable to about $\bar{x}/\bar{c} = 1.25$, or 72° from the stagnation point. In order to make the boundary layer unstable as far forward as 15° from the stagnation point, the Reynolds number has to be increased to about 520×10^6. The reference Reynolds number R_c is based on the radius of the sphere; the boundary layer over the forward portion of a sphere is, therefore, highly stable at large Reynolds numbers with respect to the Tollmien-Schlichting type of waves.

Because transition is often caused by roughness particles and because the roughness Reynolds number R_h where

$$R_h = \frac{\bar{u}_h \bar{h}}{\bar{\nu}}$$

has been shown to be significant in determining whether a roughness particle causes transition (see, for example, ref. 10), roughness Reynolds numbers were calculated. For roughness particles small enough for the velocity in the boundary layer to vary linearly with distance in the region between the wall and the top of the particle, the roughness Reynolds number is

$$R_h = \frac{\bar{u}_h \bar{h}}{\bar{\nu}} = \frac{\left(\frac{\partial \bar{u}}{\partial \bar{y}}\right)_w \bar{h}^2}{\bar{\nu}}$$

However, since, from reference 3 or 4,

$$\left(\frac{\partial \bar{u}}{\partial \bar{y}}\right)_w = \frac{\bar{U}}{\bar{\theta}} f$$

then,

$$R_h = \frac{\bar{U}\bar{f}\bar{h}^{-2}}{\bar{\theta}\bar{\nu}} = \frac{Uh^2fR_c}{\theta}$$

and because $\theta = \sqrt{\frac{Z}{R_c}}$, then

$$R_h = h^2R_c^{3/2}\frac{Uf}{\sqrt{Z}} \tag{15a}$$

Because U, f, and Z are independent of h and R_c, it follows that R_h varies as h^2 and as $R_c^{3/2}$. Equation (15a) can also be written as

$$\frac{R_h}{h^2R_c^{3/2}} = \frac{Uf}{\sqrt{Z}} \tag{15b}$$

Because the quantity $Uf/\sqrt{Z}$ depends only on the pressure distribution, a plot of the quantity $\frac{R_h}{h^2R_c^{3/2}}$ enables R_h to be calculated rapidly for any value of R_c and h for which the assumption of small height is valid. In connection with the assumption of small height it is noted that if $\bar{h} = \bar{\theta}$ the error in $\bar{u}_h$ varies from about -20 percent for a velocity profile near separation to about 14 percent for the plane stagnation-point velocity profile; the error is zero for the flat-plate velocity profile. If, however, $\bar{h} = 2\bar{\theta}$, then the error in $\bar{u}_h$ varies from about -30 percent to about 30 percent for the same velocity profiles; the error is less than 2 percent for the flat-plate velocity profile. It is, thus, advisable that $\bar{h}$ not exceed $\bar{\theta}$ unless the pressure gradient is almost zero; in this case $\bar{h}$ can be slightly larger than $2\bar{\theta}$. The variation of $\frac{R_h}{h^2R_c^{3/2}}$ with $\bar{x}/\bar{c}$ is shown in figure 4. For any fixed height h it is apparent that the maximum roughness Reynolds number occurs at a value of $\bar{x}/\bar{c}$ of about 1.0, or about 57° from the stagnation point. In order to give a clearer impression, figure 5 shows the dependence of R_h on $\bar{x}/\bar{c}$ for a value of $\bar{h}$ of 0.005 inch on a sphere of 60-inch radius at $R_c = 4.7 \times 10^6$.

Figures 1 to 4 allow the boundary-layer momentum thickness, stability, and roughness Reynolds number to be rapidly estimated for any sphere at any Reynolds number. These figures and figure 6, which gives the variation of the velocity-profile shape parameter K with $\bar{x}/\bar{c}$, can be used with the aid of references 3 and 4 to calculate all the other boundary-layer quantities.

Disk

In order to investigate the effect on the various boundary-layer parameters of an increase in bluntness, the extreme case of the flow against a disk was investigated. Because no velocity distributions $U(x)$ seem to be available for a disk, an approximate distribution was obtained by combining theoretical results with a measured distribution of U on the face of a plate of infinite span and perpendicular to the stream. The assumption was made that, at the same value of x,

$$\left(\frac{U_d}{U_p}\right)_a = \left(\frac{U_d}{U_p}\right)_{th} \tag{16}$$

The theoretical expression for U_d from reference 7 is

$$U_d = \frac{2}{\pi}\frac{x}{\sqrt{1 - x^2}}$$

and the theoretical expression for U_p from reference 7 is

$$U_p = \frac{x}{\sqrt{1 - x^2}}$$

Thus,

$$\left(\frac{U_d}{U_p}\right)_{th} = \frac{2}{\pi}$$

and

$$U_{d,a} = \frac{2}{\pi} U_{p,a} \tag{17}$$

The values of $U_{p,a}$ used were obtained from the experimental values given in figure 1 of reference 11. The variation of the approximate velocity distribution $\left(\frac{\bar{U}}{\bar{U}_\infty}\right)_d$, or U_d, with $\bar{x}/\bar{c}$ over the face of a disk perpendicular to the stream is shown in figure 7. A comparison of this velocity distribution with the calculated velocity distribution over the front face of the more forward of the two disks that are separated by a cavity (see table III and p. 106 of ref. 12) indicates that the velocity distribution shown in figure 7 is probably a good-enough approximation

to the actual velocity distribution to allow the main points to be shown by the boundary-layer analysis. In order to calculate the boundary-layer quantities of interest, a different and more rapid, although more approximate, method was used to integrate the momentum equation for the disk. The method consists in obtaining an integrated form of the momentum equation. The momentum equation (eq. (2)) can be written as

$$\frac{dZ}{dx} + \frac{2Z}{r}\frac{dr}{dx} - \frac{2}{U}\left[f - k_1 - k\left(2 + \frac{\delta^*}{\theta}\right)\right] = 0 \tag{18}$$

The quantity k is related to Z by the definition

$$k = Z\frac{dU}{dx}$$

From the relations

$$f = g\left[1 + K\left(1 - \frac{\pi}{6}\right)\right]$$

and

$$g^2(K + 1) - fk_1 - k = 0$$

(from ref. 4) it follows that

$$f = \frac{k\left(1 - \frac{\pi}{6}\right) + g^2\frac{\pi}{6}}{-k_1\left(1 - \frac{\pi}{6}\right) + g}$$

$$= \frac{Z\frac{dU}{dx}\left(1 - \frac{\pi}{6}\right) + g^2\frac{\pi}{6}}{-k_1\left(1 - \frac{\pi}{6}\right) + g} \tag{19}$$

Now, let

$$\left.\begin{aligned} &\left(1 - \frac{\pi}{6}\right) = a \\ &\frac{\pi}{6} = b \\ &g - k_1 a = C \qquad (k_1 \text{ assumed to be constant}) \\ &\frac{a}{C} = d \\ &\frac{g^2 b}{C} = e \\ &2 + \frac{\delta^*}{\theta} = A \end{aligned}\right\} \tag{20}$$

where a, b, C, d, e, and A are constants. When the definition of k, the expression for f from equation (19), and the definitions from equation (20) are substituted into equation (18), the result is

$$\frac{dZ}{dx} + 2Z\left[\frac{1}{r}\frac{dr}{dx} + \frac{A - d}{U}\frac{dU}{dx}\right] = \frac{2}{U}\left(e - k_1\right) \tag{21}$$

In this equation δ^*/θ, g, and k_1 are assumed to be constant. Equation (21) is linear in Z and is first order. Integration of equation (21) gives

$$Z = \frac{1}{r^2U^{2(A-d)}}\left[2\left(e - k_1\right)\int_{x_o}^{x} r^2U^{2(A-d)-1}\,dx + Z_o r_o^{\,2} U_o^{\,2(A-d)}\right] \tag{22}$$

When use is made of the fact that $U_o = r_o = 0$ at the stagnation point ($x = 0$) and that $Z = \theta^2 R_c$, equation (22) becomes

$$\theta\sqrt{R_c} = \frac{1}{rU^{A-d}}\left[2\left(e - k_1\right)\int_{0}^{x} r^2U^{2(A-d)-1}\,dx\right]^{1/2} \tag{23}$$

In order to find the value of $\left(\theta\sqrt{R_c}\right)_t$, note that near $x = 0$ the approximate relations $U = \left(\frac{dU}{dx}\right)_t x$ and $r = x$ are valid. Equation (23) can then be integrated with the result that

$$\left(\theta\sqrt{R_c}\right)_t = \sqrt{\frac{e - k_1}{\left(\frac{dU}{dx}\right)_t (A - d + 1)}} \tag{24}$$

Equation (24) indicates that, in the region in which the relations $U = \left(\frac{dU}{dx}\right)_t x$ and $r = x$ are approximately valid, the boundary-layer thickness is approximately constant. It is clear that in this region $\theta\sqrt{R_c}$ is proportional to $\frac{1}{\sqrt{\left(\frac{dU}{dx}\right)_t}}$. In figure 8 is shown the variation of $\frac{\bar{\theta}}{\bar{c}}\sqrt{R_c}$ with $\bar{x}/\bar{c}$ calculated by use of equations (23) and (24) together with $k_1 = 0$ and stagnation-point values for $A - d$ and e; these values are

$$\left.\begin{aligned} A - d &= 3.3407 \\ e &= 0.23002 \end{aligned}\right\} \tag{25}$$

The variation of the boundary-layer Reynolds number R_θ and the critical Reynolds number $R_{\theta,c}$ with $\bar{x}/\bar{c}$ is shown, respectively, in figures 9 and 10. The values of $R_{\theta,c}$ were calculated by first computing the values of k from

$$k = Z \frac{dU}{dx}$$

where $Z = \theta^2 R_c$, then by reading the value of K for each value of k from a large-sized plot of K against k, and then by reading the value of $R_{\theta,c}$ from a large-sized plot of $R_{\theta,c}$ against K. Small plots of K against k and of $R_{\theta,c}$ against K are given in reference 4.

The most striking results are that the boundary-layer thickness is greatest at the stagnation point and decreases with an increase in distance from this point and that the boundary layer is completely stable at a Reynolds number of 4.7×10^6, based on the radius of the disk. The smallest Reynolds number for which the boundary layer will first become unstable is about 720×10^6; the first unstable point will occur at about $x = 0.75$. It is apparent that the boundary layer on a disk is very stable with respect to the Tollmien-Schlichting type of waves.

In order to investigate the variation of roughness Reynolds number over the disk, the quantity $\frac{R_h}{h^2 R_c^{3/2}}$ was calculated. The results are shown in figure 11. In figure 12 is shown the dependence of R_h on $\bar{x}/\bar{c}$ for a value of $\bar{h}$ of 0.005 inch on a disk of 60-inch radius at $R_c = 4.7 \times 10^6$. A comparison of figure 12 with figure 5 shows that the maximum value of R_h produced on a disk is less than that produced on a sphere when the roughness height is the same for disk and sphere. A comparison of figures 5 and 12 also indicates that a roughness of given height produces a given roughness Reynolds number over a greater portion of the sphere than of the disk. This result follows from the fact that, for a given height of roughness and with the sphere and disk having the same diameter and Reynolds number, the maximum roughness Reynolds number on the sphere is larger than that on the disk and occurs near $\bar{x}/\bar{c} = 1.0$ (near 57° from the stagnation point) on the sphere but at the edge of the disk. If the same roughness height is present on the sphere and disk and if the reference Reynolds number is increased, a critical value of R_h will occur at

a lower reference Reynolds number on the sphere than on the disk and will occur farther forward on the sphere than on the disk. (See ref. 10 for information concerning critical values of R_h.)

ACCURACY OF RESULTS

In order to determine the accuracy of equation (23), the quantity $\frac{\bar{\theta}}{\bar{c}}\sqrt{R_c}$ for the sphere was calculated for $k_1 = 0$ and with stagnation-point values of $A - d$ and e; in figure 13 the results are compared with the results of the step-by-step integration of the momentum equation for the sphere. The agreement is very good not too near the separation point. For small values of $\bar{x}/\bar{c}$ it is difficult to compute accurate values of $\frac{\bar{\theta}}{\bar{c}}\sqrt{R_c}$ by the use of equation (23) because both numerator and denominator become very small. In this region it is advisable to make use of equation (24) as an aid in obtaining values of $\frac{\bar{\theta}}{\bar{c}}\sqrt{R_c}$.

If the values of $A - d$ and e for a flat plate parallel to the flow $\left(\frac{dU}{dx} = 0\right)$ are used, the values of $A - d$ and e, respectively, are then

$$A - d = 3.5$$

and

$$e = 0.2145 \qquad (k_1 = 0)$$

With this value of $A - d$ and the fact that $r = \sin x$ and $U = \frac{3}{2}\sin x$, equation (23) can be integrated in closed form for the sphere with the result that

$$\theta\sqrt{R_c} = \frac{0.53492}{(\sin x)^{4.5}}\left[\frac{105}{384}x - \frac{\cos x}{8}\left(\sin^7 x + \frac{7}{6}\sin^5 x + \frac{35}{24}\sin^3 x + \frac{105}{48}\sin x\right)\right]^{1/2} \tag{26}$$

A different closed-form integral of equation (23), which is given in reference 1, can be obtained from equation (23) by letting

$$A - d = 3$$

and

$$e = 0.2222 \qquad \left(k_1 = 0\right)$$

The results of equation (26) are also shown in figure 13. Better agreement is obtained with the more exact step-by-step method of integration if the stagnation-point values of $A - d$ and e are used in a region of falling pressure. Therefore, the values of equation (25) are used together with equation (23) to calculate the boundary-layer parameters on the disk.

It may be worthwhile to note that equation (23) for the estimation of the boundary-layer momentum thickness is general in the sense that the constants e, $A - d$, and k_1 are arbitrary. Therefore, the accuracy of a result can be improved by choosing values of the constants that are appropriate for the type of pressure distribution under consideration. (see table 2 of ref. 3 for suitable values.) One example of the effect of the choice of the constants is shown in figure 13. By making use of an average value of k_1, equation (23) also permits a rough estimate to be made of the effect on the boundary-layer thickness of flow into or out of the surface.

An indication of the accuracy of the calculated values of the boundary-layer thickness on both the sphere and the disk can be obtained from the exact solution for the boundary layer at the stagnation point of a body of revolution at zero angle of attack. This exact nondimensional velocity profile is known to be the same as the velocity profile on the wedge with $\beta = \frac{1}{2}$ (p. 129 of ref. 9). Following the notation of reference 2 and letting $\beta = \frac{1}{2}$ gives

$$\bar{\theta}_t = \sqrt{\frac{\bar{\nu}}{2\left(\frac{d\bar{U}}{d\bar{x}}\right)_t}}\left[\int_0^\infty F'(1 - F')dY\right]_{\beta=\frac{1}{2}}$$

or, with (see table II of ref. 2)

$$\left[\int_0^\infty F'(1 - F')dY\right]_{\beta=\frac{1}{2}} = 0.3502$$

the result is

$$\left(\theta\sqrt{R_c}\right)_t = \frac{0.2476}{\sqrt{\left(\frac{dU}{dx}\right)_t}} \tag{27}$$

The result obtained from substituting $k_1 = 0$ and stagnation-point values from equation (25) into equation (24) is

$$\left(\theta\sqrt{R_c}\right)_t = \frac{0.2302}{\sqrt{\left(\frac{dU}{dx}\right)_t}} \tag{28}$$

The error in equation (28) is about 7.5 percent. From this result it seems reasonable to infer that in the region of falling pressure the boundary-layer thickness, boundary-layer Reynolds number, and roughness Reynolds number are probably accurate to within approximately 10 percent.

When, however, the accuracy of the critical Reynolds number $R_{\theta,c}$ is examined, the conclusion is reached that the calculated values of the critical Reynolds numbers can easily differ from the correct values by as much as 100 percent. Thus, from table II of reference 2 the value 2,662 is obtained for $R_{\theta,c}$ at the stagnation point. The value of $R_{\theta,c}$ obtained from the present analysis is 1,650, a difference of about 60 percent. Both calculations of $R_{\theta,c}$ use the rapid method employed in reference 13; the difference in the two values of $R_{\theta,c}$ is caused by the different velocity profiles: one is the exact and the other is the approximate Schlichting profile. When it is noted that the rapid method of reference 13 yields approximate answers, the conclusion is reached that the values of $R_{\theta,c}$ given in the present analysis can easily differ from the correct values by as much as 100 percent. The conclusions reached in the analysis concerning the stability, however, still remain the same in a qualitative sense.

CONCLUDING REMARKS

The calculations for the sphere show that the boundary layer at the stagnation point of a sphere is much thicker than that on an airfoil, that the boundary-layer thickness increases very slowly with an increase in distance from the stagnation point, that the boundary layer over the forward portion of a sphere is highly stable at large Reynolds numbers with respect to the Tollmien-Schlichting type of waves, and that roughness of a given height produces the largest roughness Reynolds numbers at about 57° from the stagnation point.

The calculations for the disk show the unusual result that the boundary-layer thickness is greatest at the stagnation point and decreases with an increase in distance from this point, that the boundary layer is extremely stable with respect to the Tollmien-Schlichting type of waves, and that roughness of a given height produces a given roughness Reynolds number over a smaller portion of the disk surface than over the sphere surface.

Langley Aeronautical Laboratory,
National Advisory Committee for Aeronautics,
Langley Field, Va., June 9, 1958.

REFERENCES

1. Hsu, E. Y., and Macovsky, M. S.: Measurement of Transition on a Sphere at High Reynolds Numbers. Rep. 1110, David Taylor Model Basin, Navy Dept., June 1957.

2. Tetervin, Neal: A Study of the Stability of the Incompressible Laminar Boundary Layer on Infinite Wedges. NACA TN 2976, 1953.

3. Schlichting, H.: An Approximate Method for Calculation of the Laminar Boundary Layer With Suction for Bodies of Arbitrary Shape. NACA TM 1216, 1949.

4. Tetervin, Neal, and Levine, David A.: A Study of the Stability of the Laminar Boundary Layer As Affected by Changes in the Boundary-Layer Thickness in Regions of Pressure Gradient and Flow Through the Surface. NACA TN 2752, 1952.

5. Tetervin, Neal, and Lin, Chia Chiao: A General Integral Form of the Boundary-Layer Equation For Incompressible Flow With an Application to the Calculation of the Separation Point of Turbulent Boundary Layers. NACA Rep. 1046, 1951. (Supersedes NACA TN 2158.)

6. Milne, William Edmund: Numerical Calculus. Princeton Univ. Press, 1949, p. 121.

7. Milne-Thomson, L. M.: Theoretical Hydrodynamics. Macmillan and Co., Ltd., 1938.

8. Fluid Motion Panel of the Aeronautical Research Committee and Others: Modern Developments in Fluid Dynamics. Vol. II, S. Goldstein, ed., The Clarendon Press (Oxford), 1938, p. 497.

9. Schlichting, Hermann (J. Kestin, trans.): Boundary Layer Theory. McGraw-Hill Book Co., Inc., 1955.

10. Von Doenhoff, Albert G., and Horton, Elmer A.: A Low-Speed Experimental Investigation of the Effect of a Sandpaper Type of Roughness on Boundary-Layer Transition. NACA Rep. 1349, 1958. (Supersedes NACA TN 3858.)

11. Roshko, Anatol: A New Hodograph for Free-Streamline Theory. NACA TN 3168, 1954.

12. Garabedian, P. R.: Calculation of Axially Symmetric Cavities and Jets. Tech. Rep. No. 42 (Contract Nonr-225(11)), Appl. Math. and Statistics Lab., Stanford Univ., Sept. 30, 1955.

13. Lin, C. C.: On the Stability of Two-Dimensional Parallel Flows. Part III. Stability in a Viscous Fluid. Quarterly Appl. Math., vol. III, no. 4, Jan. 1946, pp. 277-301.

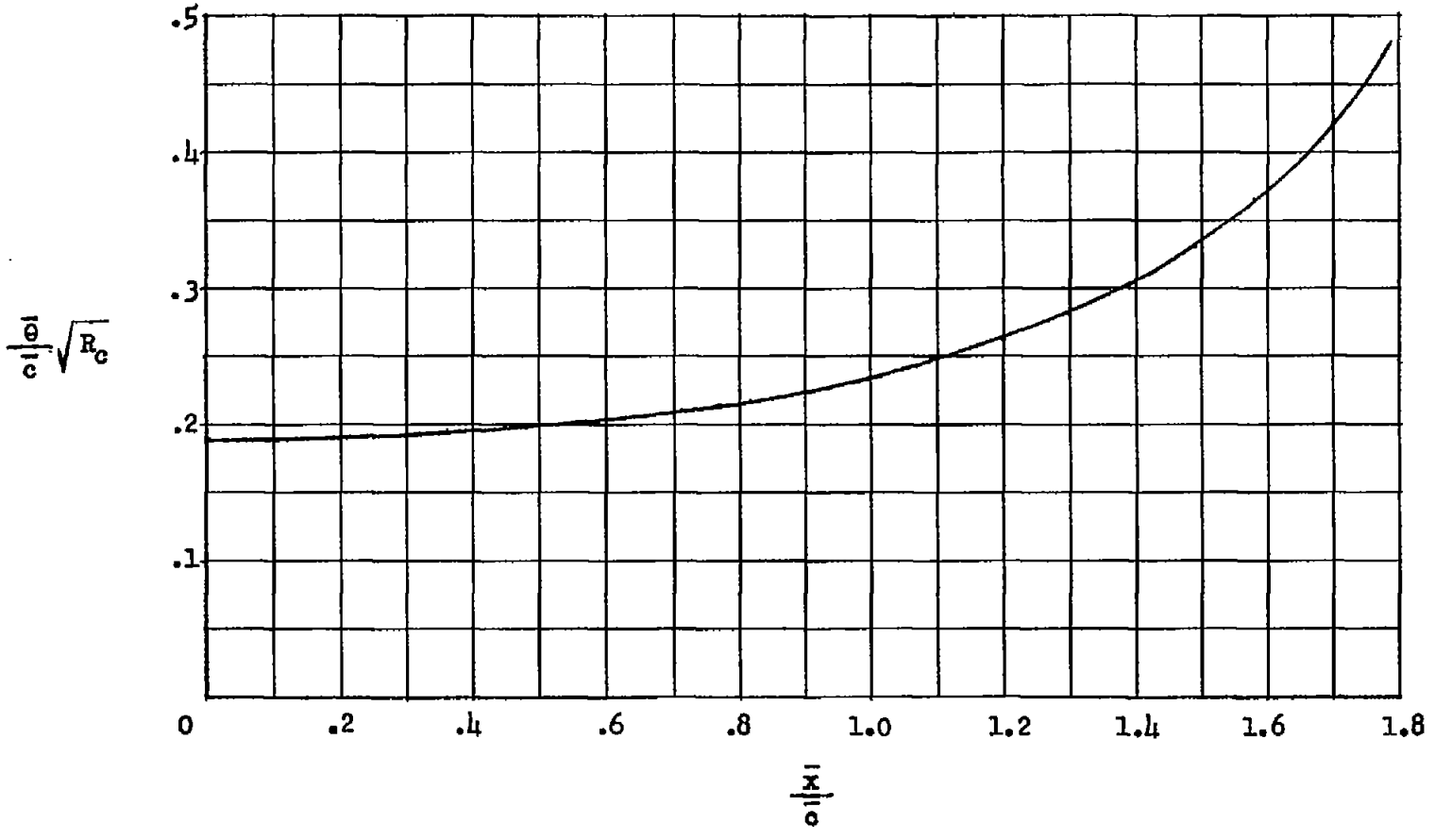

Figure 1.- Variation of nondimensional boundary-layer thickness $\frac{\bar{\theta}}{\bar{c}}\sqrt{R_c}$ with $\bar{x}/\bar{c}$ for a sphere.

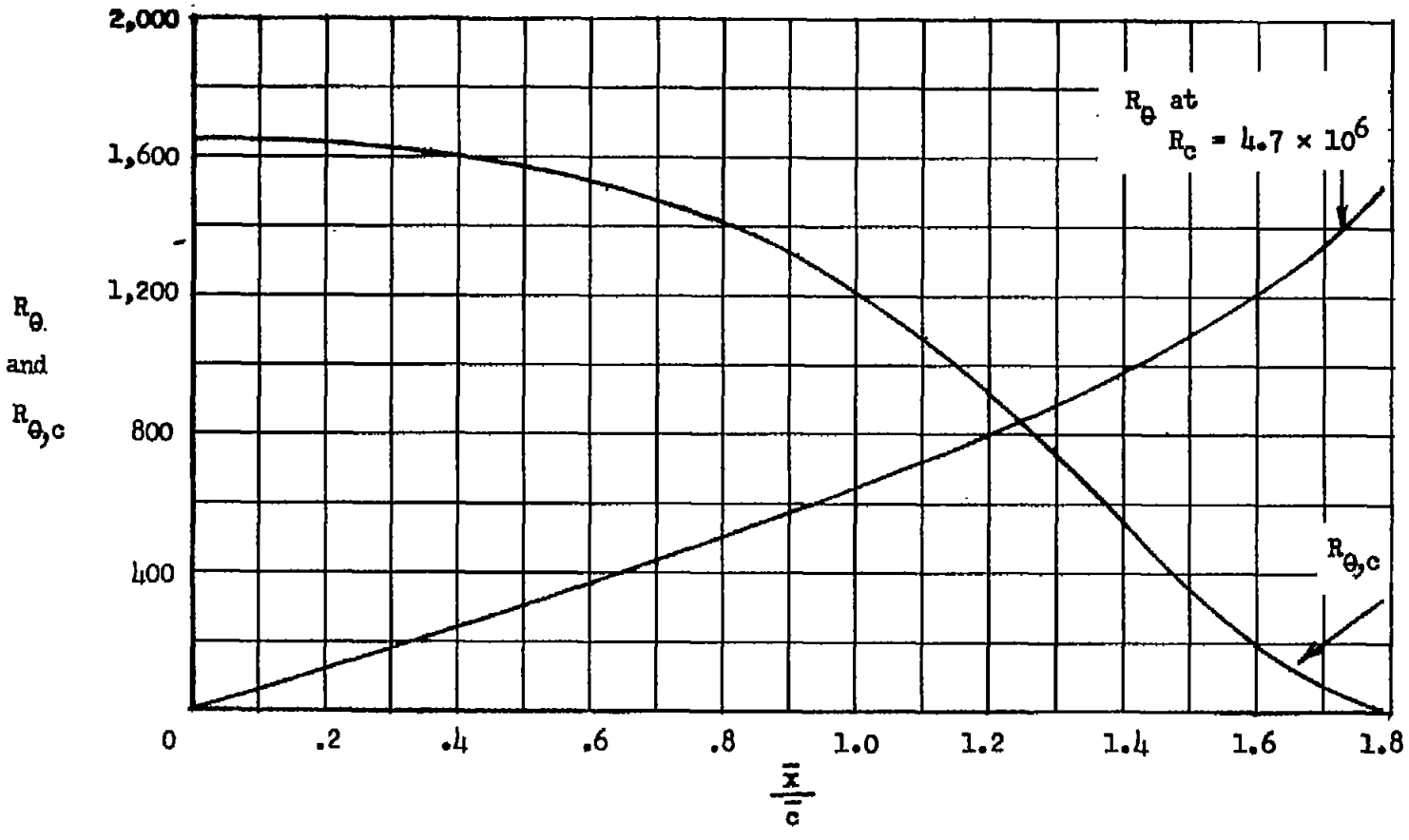

Figure 2.- Variation of boundary-layer Reynolds number R_θ and of boundary-layer minimum critical Reynolds number $R_{\theta,c}$ with $\bar{x}/\bar{c}$ for a sphere.

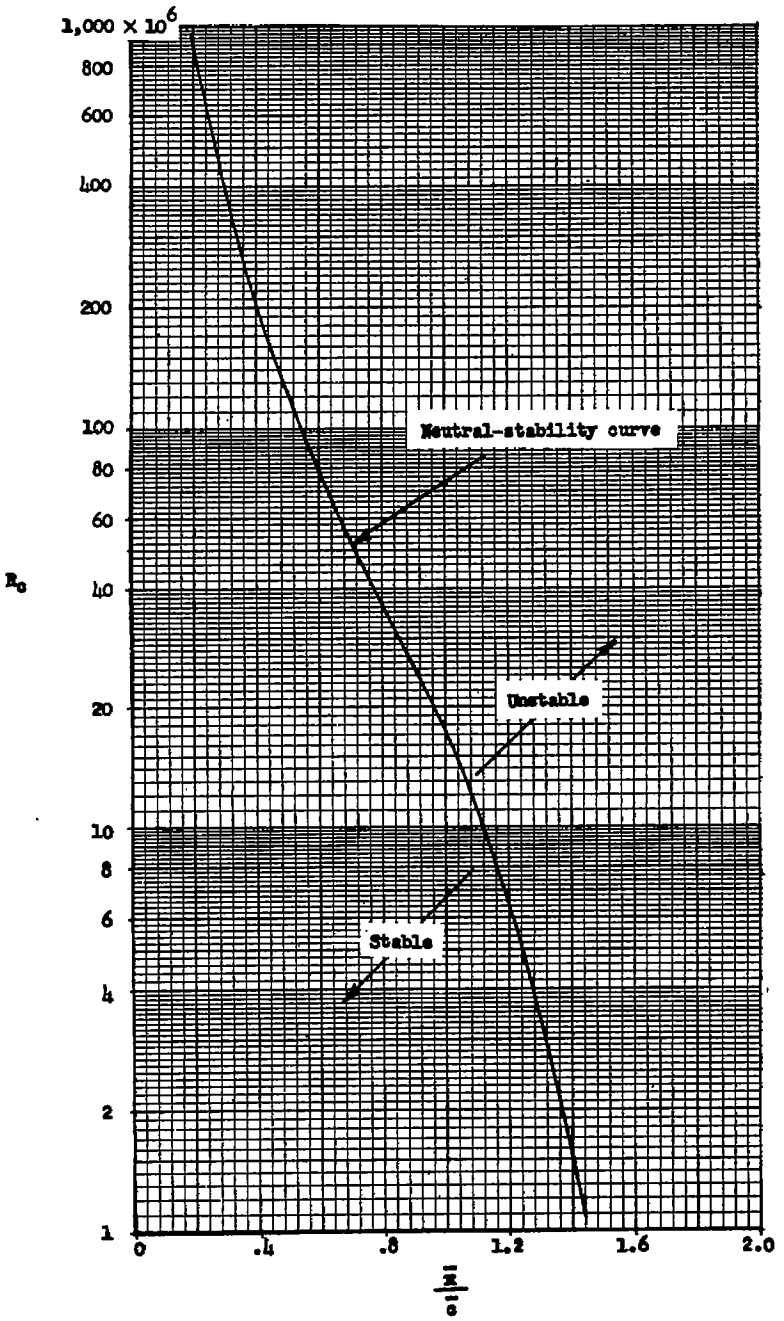

Figure 3.- Value of Reynolds number R_c for neutral stability $\left(R_\theta = R_{\theta,c}\right)$ at any value of $\bar{x}/\bar{c}$ on a sphere.

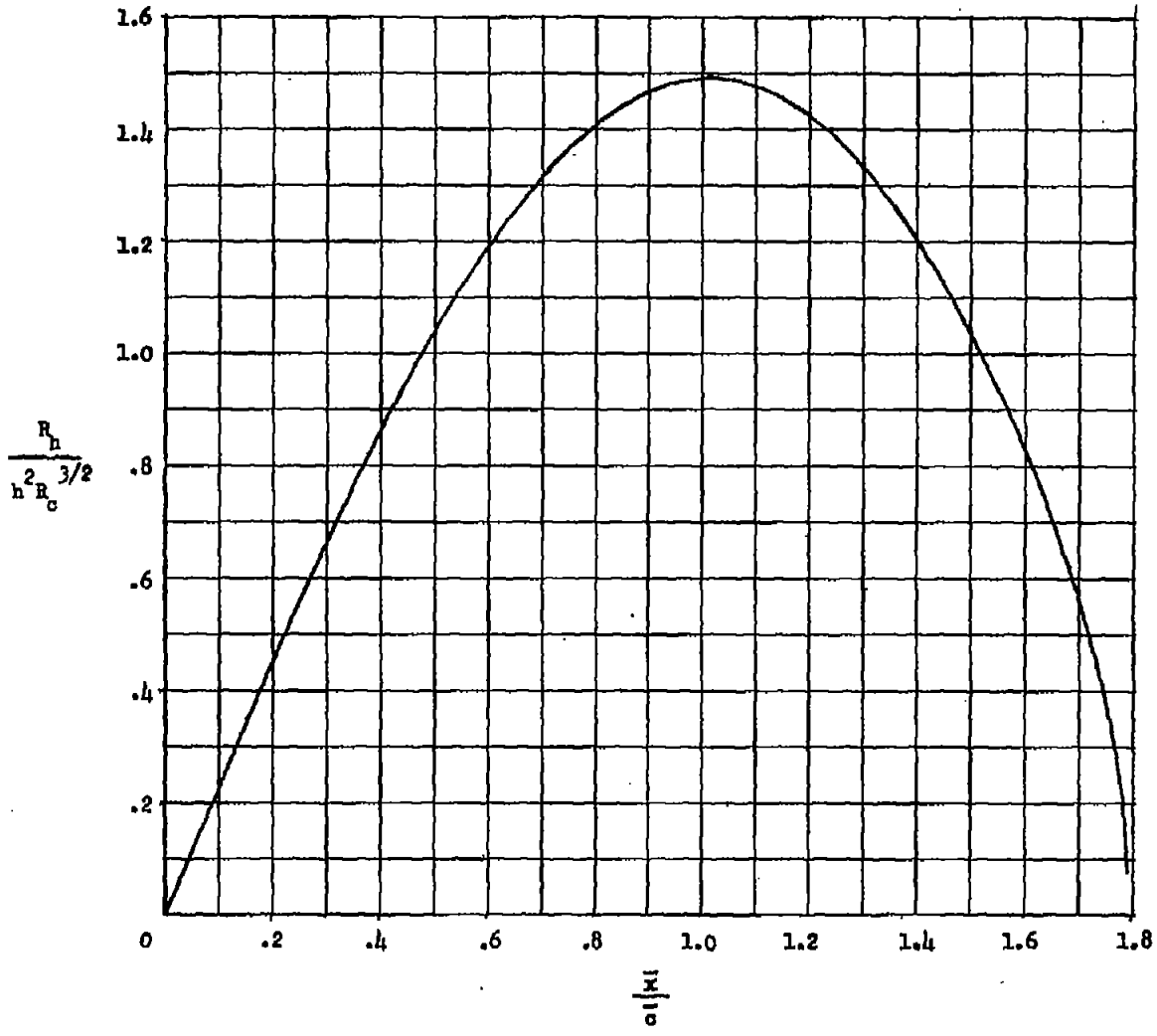

Figure 4.- Variation of roughness Reynolds number parameter $\frac{R_h}{h^2 R_c^{3/2}}$ with $\bar{x}/\bar{c}$ for a sphere.

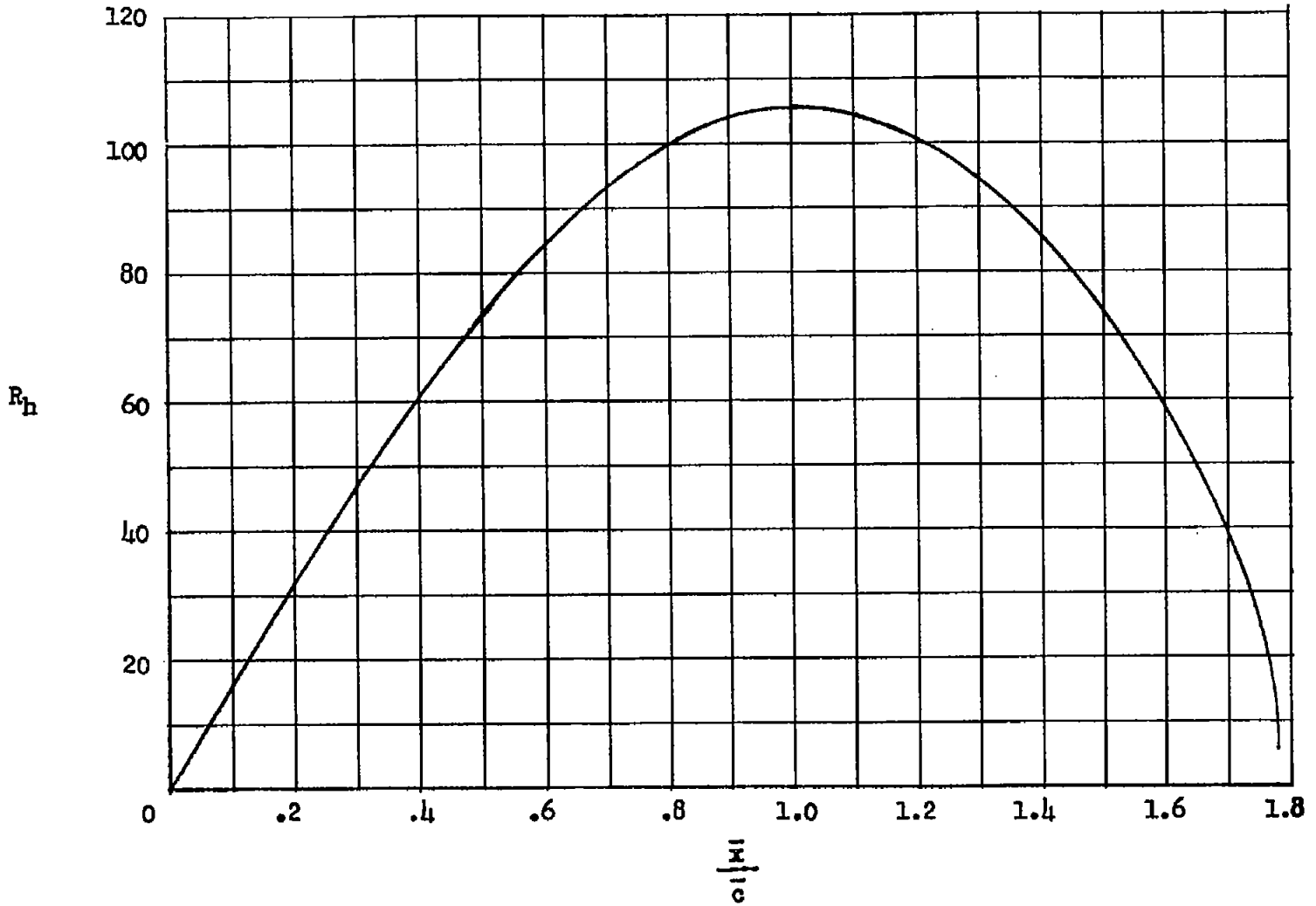

Figure 5.- Dependence of R_h on $\bar{x}/\bar{c}$ for $\bar{h}$ = 0.005 inch at $\bar{x}/\bar{c}$ on a sphere of 60-inch radius at $R_c = 4.7 \times 10^6$.

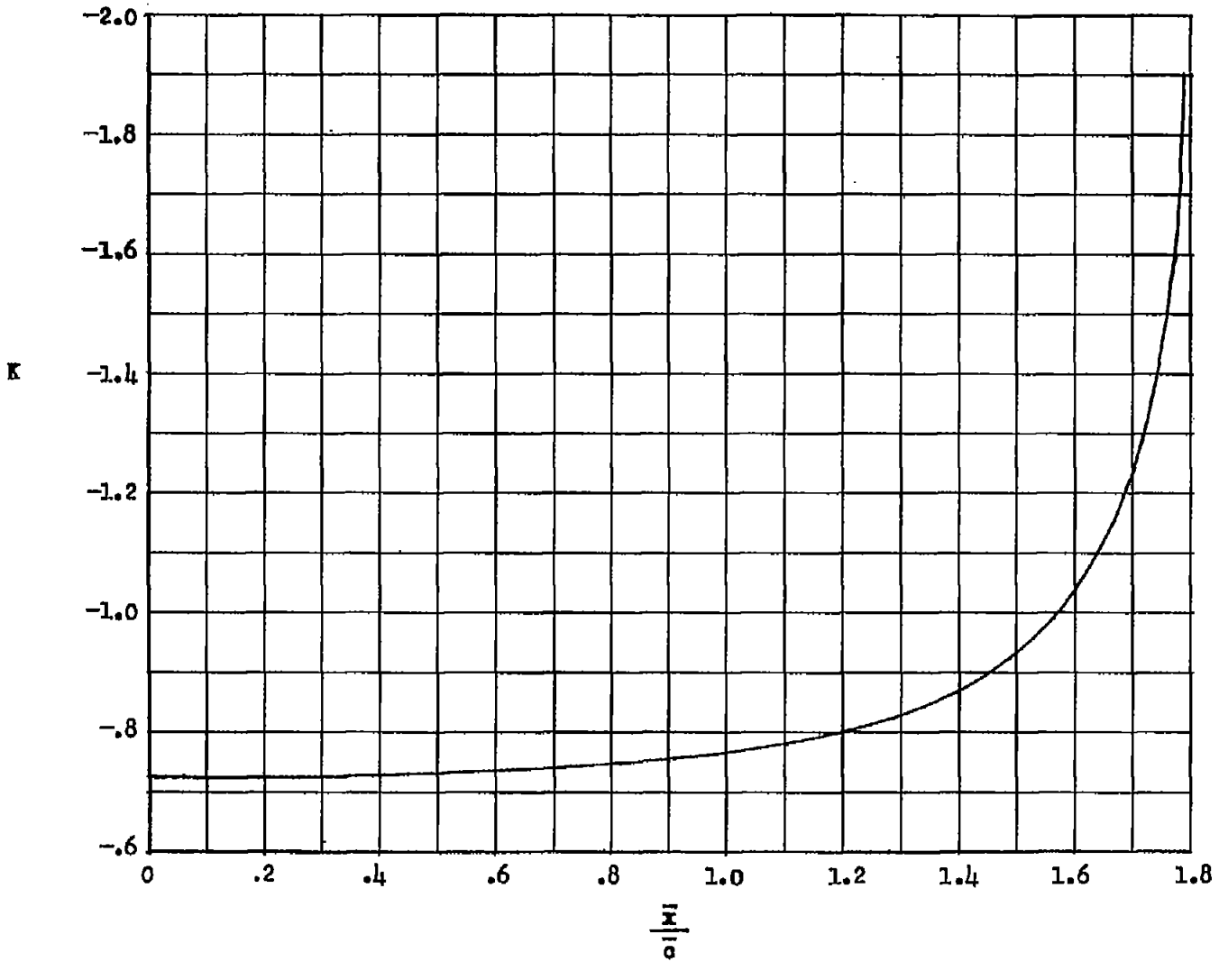

Figure 6.- Variation of velocity-profile shape parameter K with $\bar{x}/\bar{c}$ for a sphere.

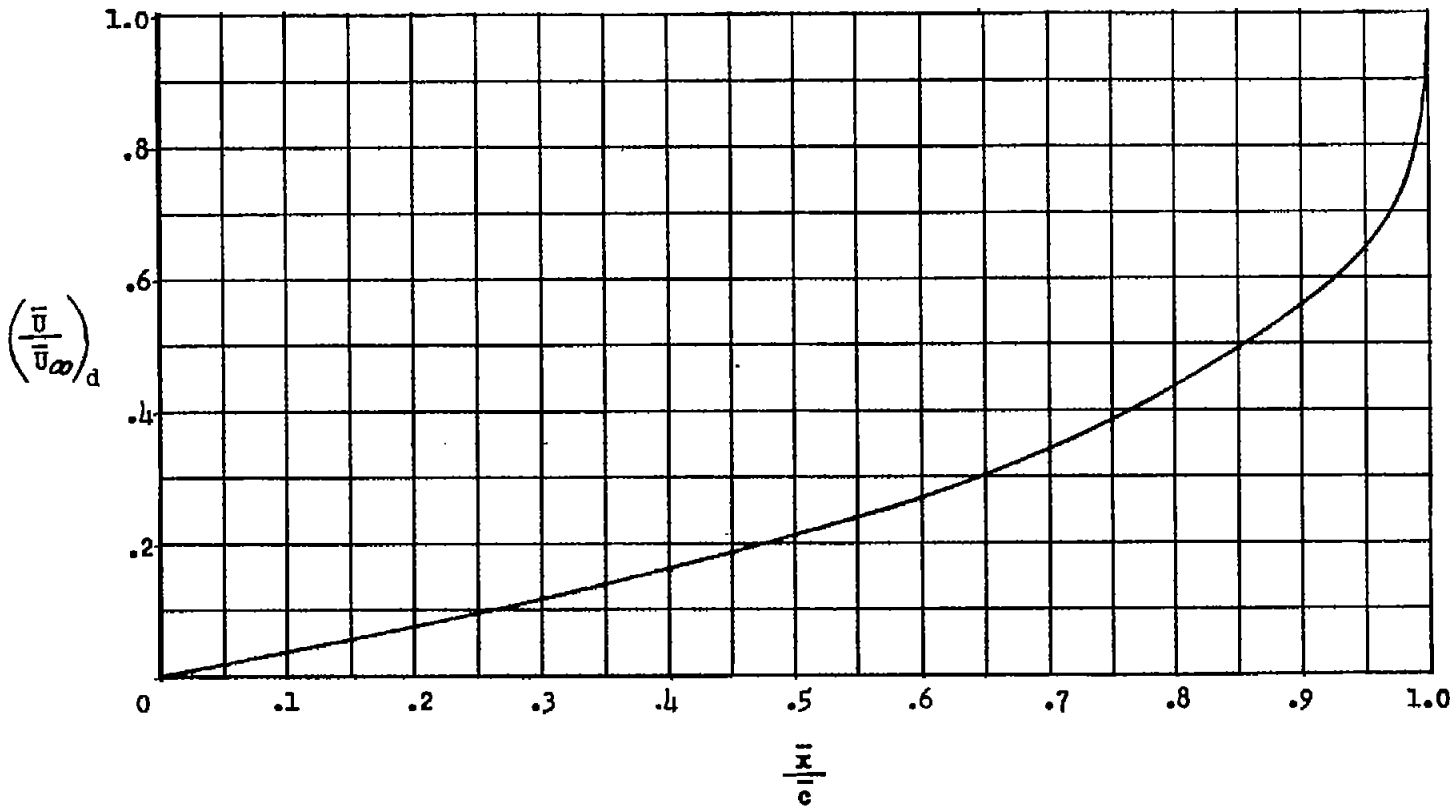

Figure 7.- Variation of approximate velocity distribution $\left(\frac{\bar{U}}{\bar{U}_\infty}\right)_d$ with $\bar{x}/\bar{c}$ on the face of disk perpendicular to the stream.

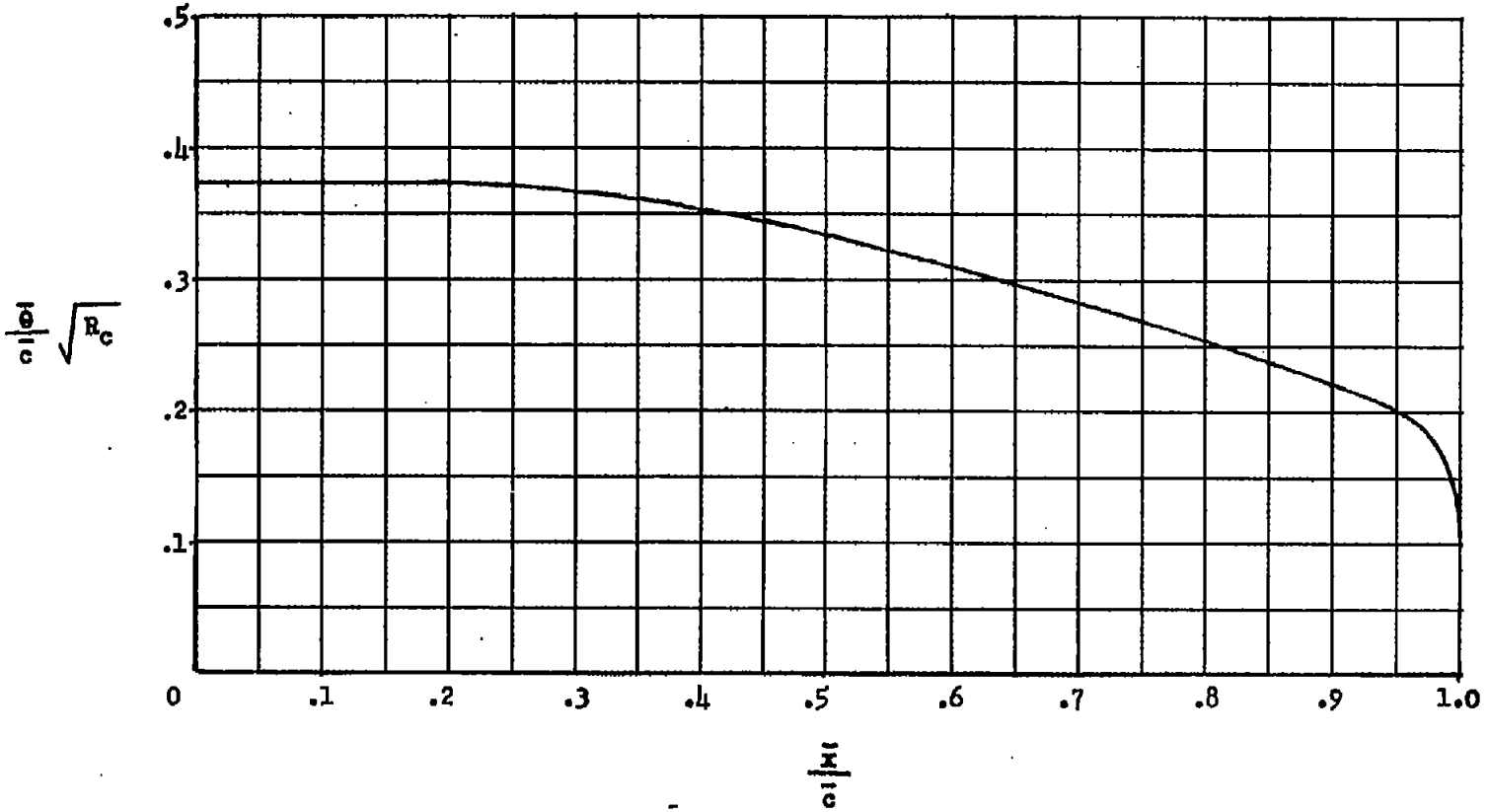

Figure 8.- Variation of $\frac{\bar{\theta}}{\bar{c}}\sqrt{R_c}$ with $\bar{x}/\bar{c}$ on the face of a disk perpendicular to the stream.

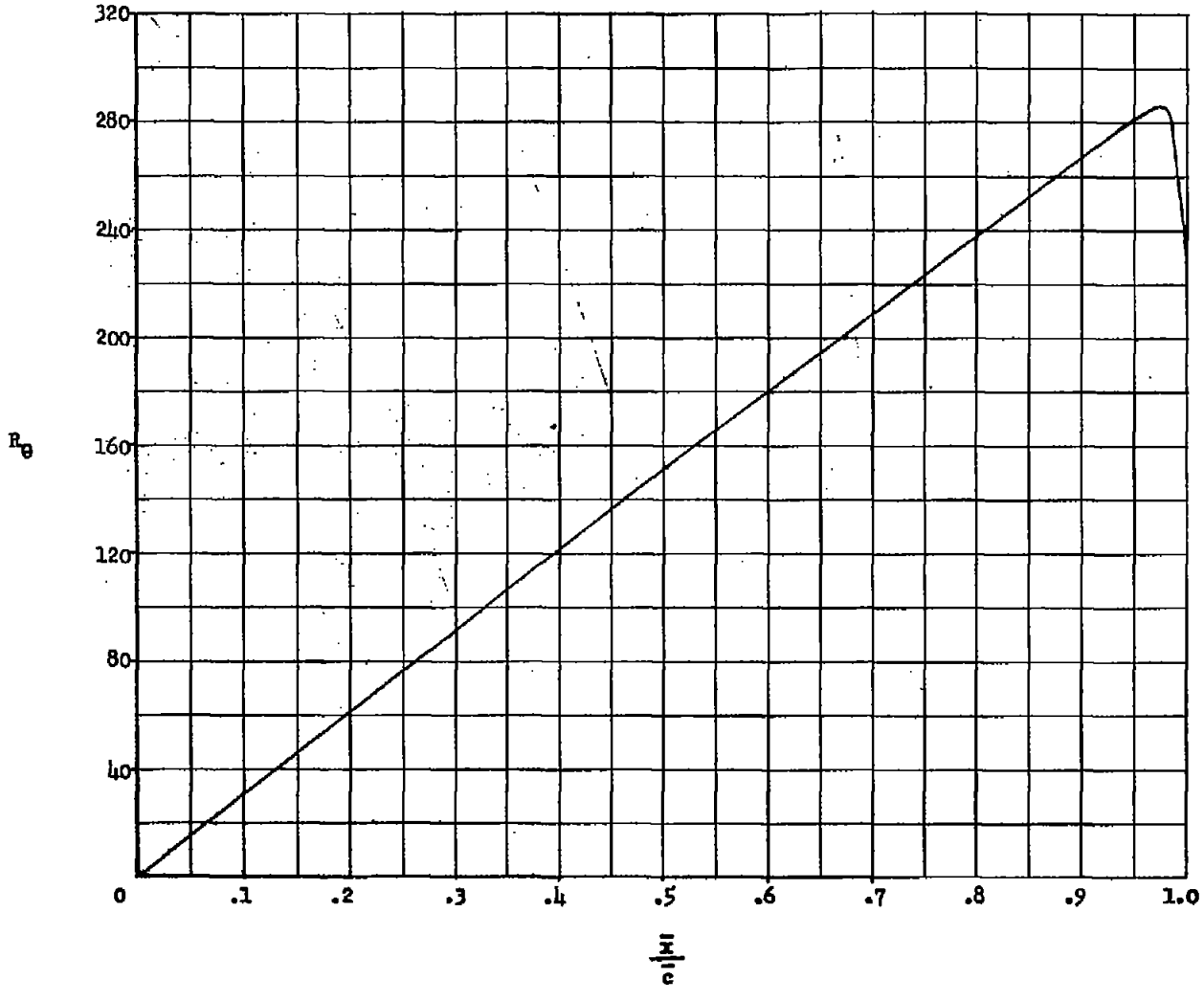

Figure 9.- Variation of R_θ with $\bar{x}/\bar{c}$ on the face of a disk perpendicular to the stream at $R_c = 4.7 \times 10^6$.

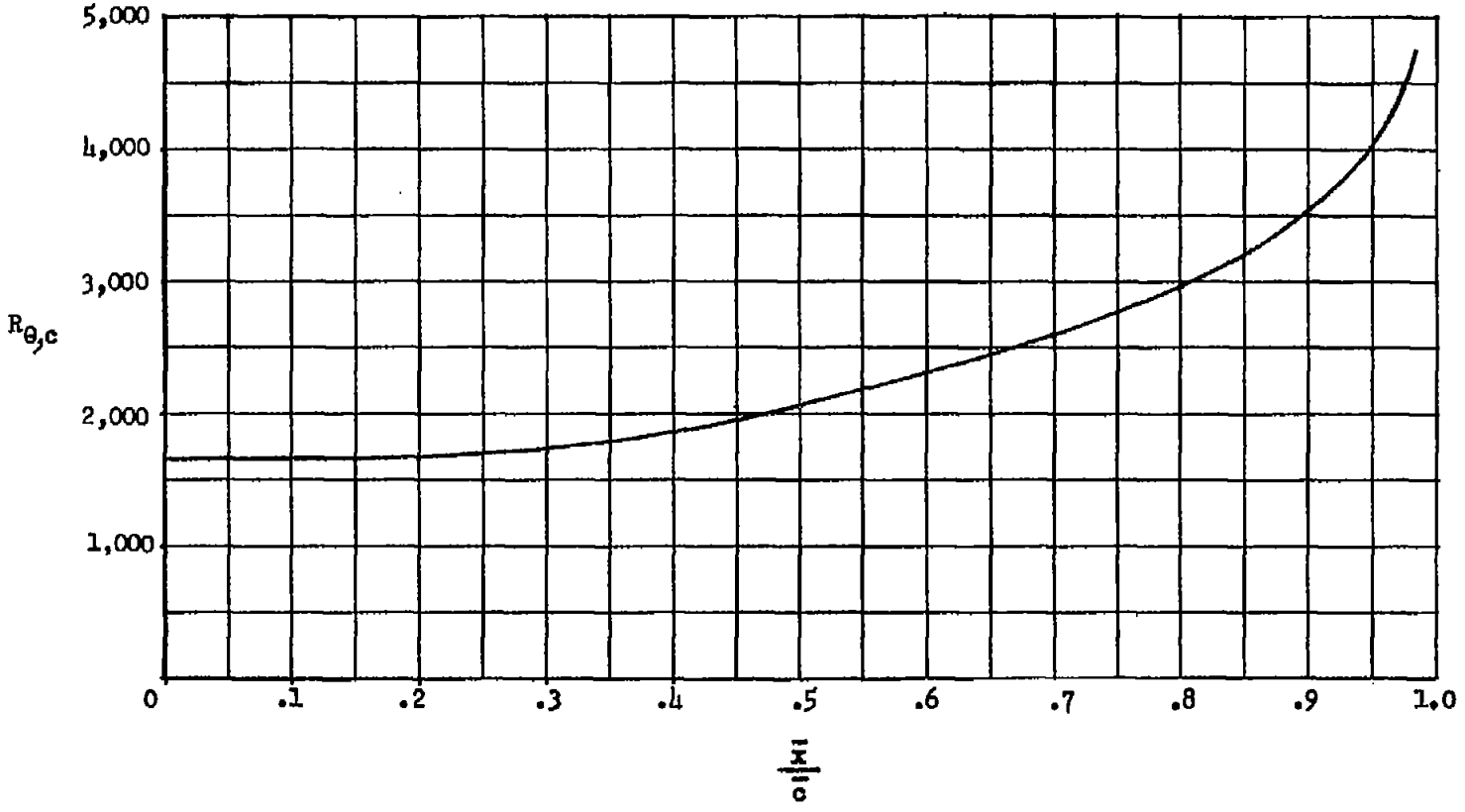

Figure 10.- Variation of $R_{\theta,c}$ with $\bar{x}/\bar{c}$ on the face of a disk perpendicular to the stream.

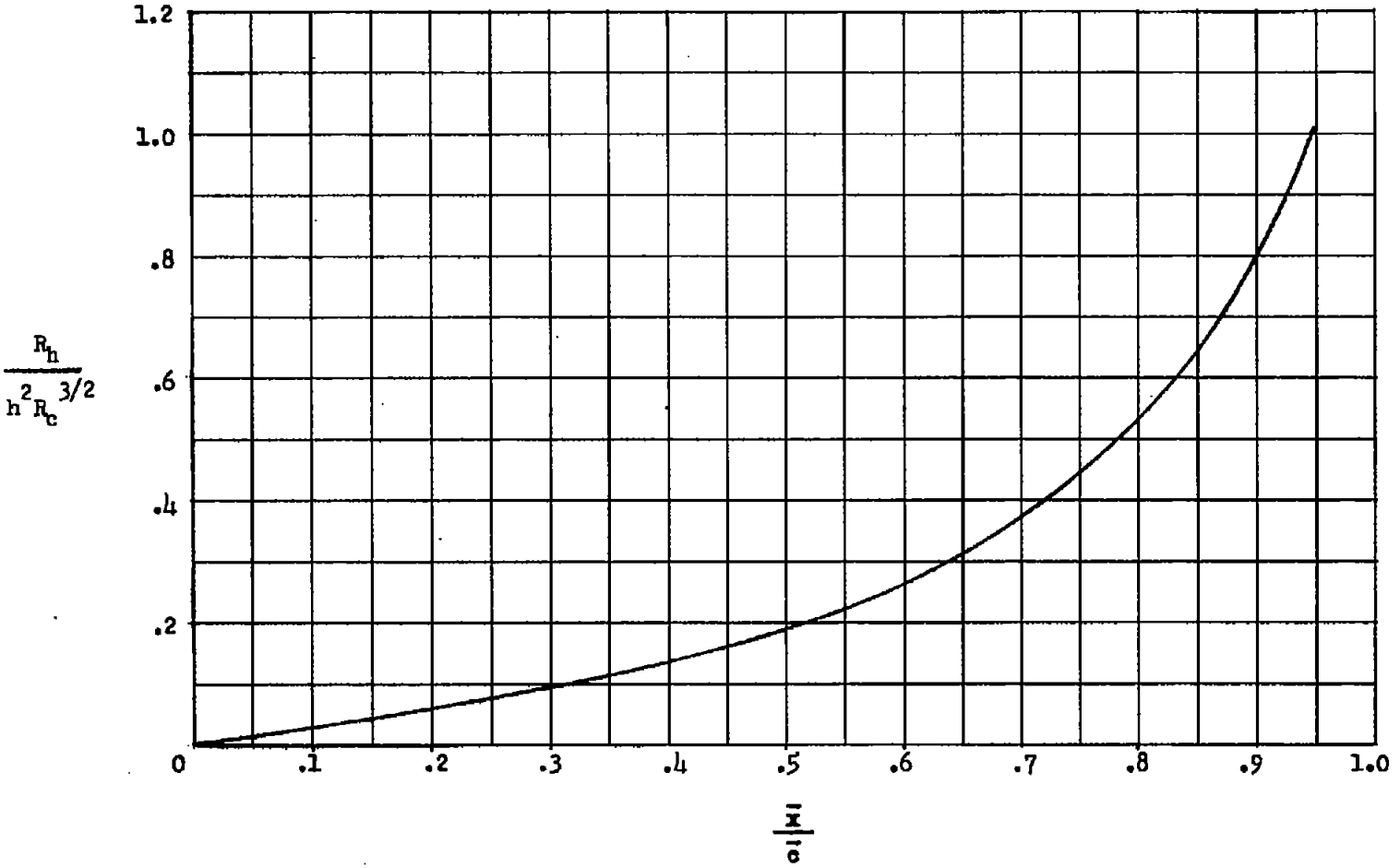

Figure 11.- Variation of roughness Reynolds number parameter $\frac{R_h}{h^2 R_c^{3/2}}$ with $\bar{x}/\bar{c}$ for a disk.

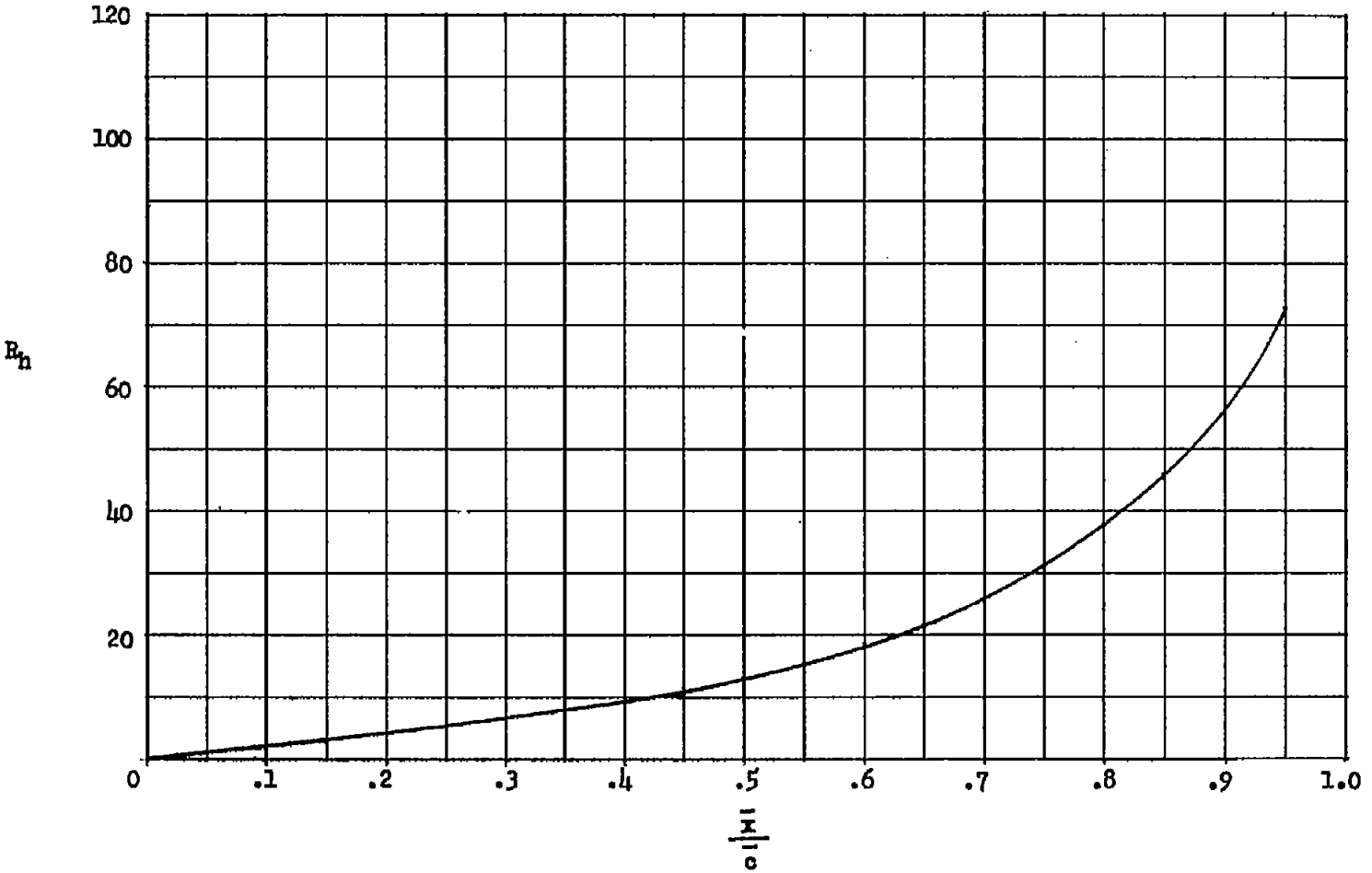

Figure 12.- Dependence of R_h on $\bar{x}/\bar{c}$ for $\bar{h}$ = 0.005 inch at $\bar{x}/\bar{c}$ on a disk of 60-inch radius at $R_c = 4.7 \times 10^6$.

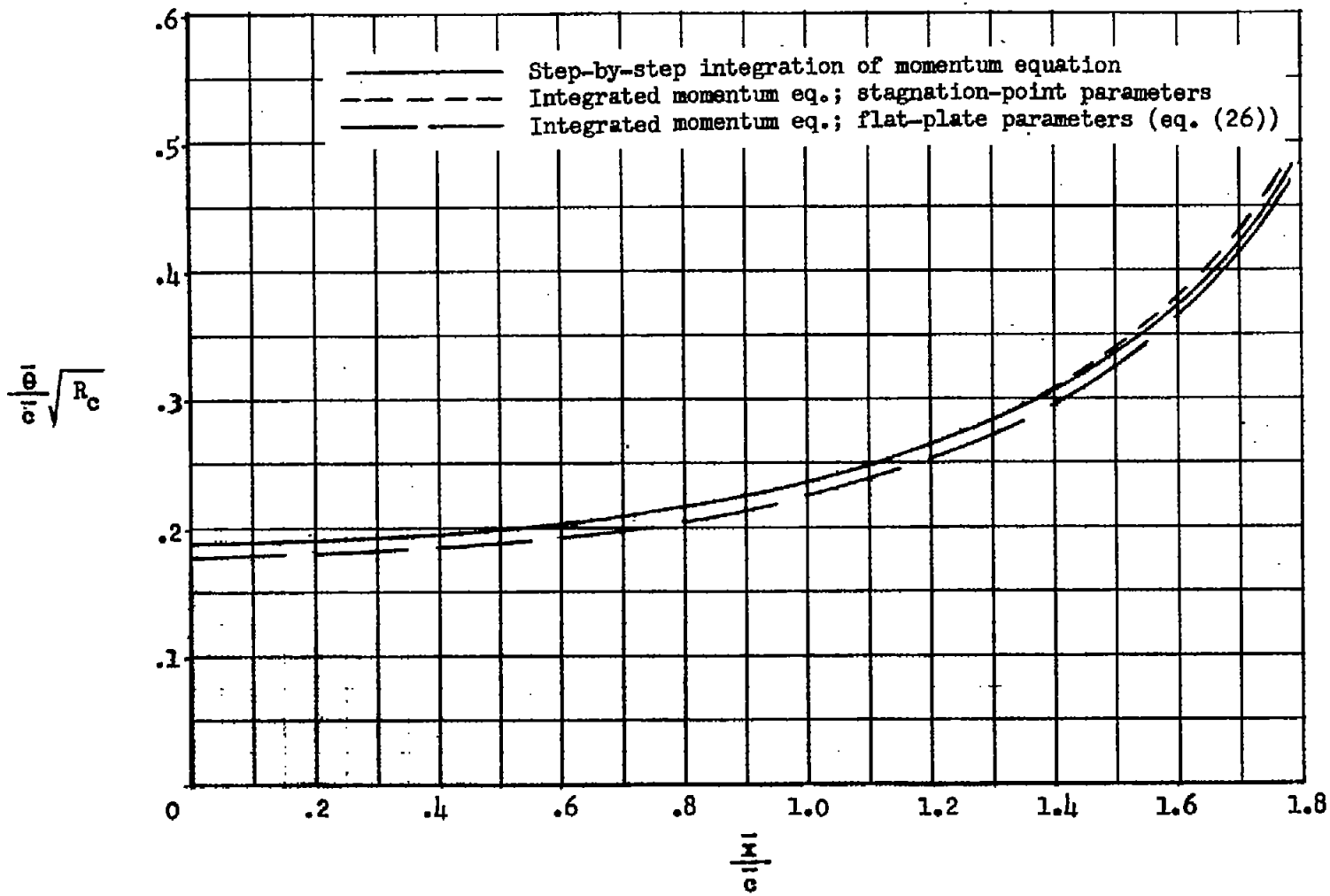

Figure 13.- Comparison of three methods of integration of the momentum equation for a sphere.

NACA - Langley Field, Va.